Australian Journal of Earth Sciences (2001) **48**, 395–408

$^{40}Ar/^{39}Ar$ and K–Ar age constraints on the timing of regional deformation, south coast of New South Wales, Lachlan Fold Belt: problems and implications*

C. L. FERGUSSON[1†] AND D. PHILLIPS[2]

[1]*School of Geosciences, University of Wollongong, NSW 2522, Australia.*
[2]*Research School of Earth Sciences, Australian National University, ACT 0200, Australia.*

Four slate samples from subduction complex rocks exposed on the south coast of New South Wales, south of Batemans Bay, were analysed by K–Ar and $^{40}Ar/^{39}Ar$ step-heating methods. One sample contains relatively abundant detrital muscovite flakes that are locally oblique to the regional cleavage in the rock, whereas the remaining samples appear to contain sparse detrital muscovite. Separates of detrital muscovite yielded plateau ages of 505 ± 3 Ma and 513 ± 3 Ma indicating that inheritance has not been eliminated by metamorphism and recrystallisation. Step-heating analyses of whole-rock chips from all four slate samples produced discordant apparent age spectra with 'saddle shapes' following young apparent ages at the lowest temperature increments. Elevated apparent ages associated with the highest temperature steps are attributed to the presence of variable quantities of detrital muscovite (<1–5%). Two whole-rock slate samples yielded similar $^{40}Ar/^{39}Ar$ integrated ages of *ca* 455 Ma, which are some 15–30 million years older than K–Ar ages for the same samples. These discrepancies suggest that the slates have also been affected by recoil loss/redistribution of ^{39}Ar, leading to anomalously old $^{40}Ar/^{39}Ar$ ages. Two other samples, from slaty tectonic mélange and intensely cleaved slate, yielded average $^{40}Ar/^{39}Ar$ integrated ages of *ca* 424 Ma, which are closer to associated mean K–Ar ages of 423 ± 4 Ma and 409 ± 16 Ma, respectively. Taking into account the potential influences of recoil loss/redistribution of ^{39}Ar and inheritance, the results from the latter samples suggest a maximum age of *ca* 440 Ma for deformation/metamorphism. The current results indicate that recoil and inheritance problems may also have affected whole-rock $^{40}Ar/^{39}Ar$ data reported from other regions of the Lachlan Fold Belt. Therefore, until these effects are adequately quantified, models for the evolution of the Lachlan Fold Belt, that are based on such whole-rock $^{40}Ar/^{39}Ar$ data, should be treated with caution.

KEY WORDS: argon–argon dating, deformation, Lachlan Fold Belt, New South Wales, potassium–argon dating, subduction.

INTRODUCTION

The Lachlan Fold Belt is well known for its complex deformational history, with a number of orogenic events and associated structural styles recognised. Recent syntheses of this orogenic evolution have emphasised the difficulty of identifying fold-belt-wide deformational episodes and have inferred the existence of diachronous deformation zones with an overall merging of episodic orogenic events (Gray & Foster 1997; Gray *et al.* 1997). $^{40}Ar/^{39}Ar$ ages have been utilised in an attempt to clarify the timing of deformation in the Lachlan Fold Belt because, in many areas, stratigraphic constraints are either absent or too broad to permit precise timing of individual deformation events (Foster *et al.* 1998, 1999; Offler *et al.* 1998; Bierlein *et al.* 1999). Debate over the implications of the $^{40}Ar/^{39}Ar$ age data has focused on the interpretation of deformation models that are at least partly constrained by the radiometric ages. Dispute has been mainly over diachronous deformation related to subduction complex settings versus episodic deformation in a convergent margin setting (VandenBerg 1999).

A significant proportion of the $^{40}Ar/^{39}Ar$ data derives from step-heating analyses of low-grade, whole-rock slates, mostly from the western Lachlan Fold Belt (Foster *et al.* 1998, 1999). Studies of similar samples from the eastern extremity of the Lachlan Fold Belt are limited to the study by Offler *et al.* (1998), who reported $^{40}Ar/^{39}Ar$ ages of 450 ± 3 Ma and 445 ± 2 Ma from samples in the Ordovician turbidite succession near Narooma and Bermagui, respectively. These ages were regarded as a precise constraint on the timing of intense underplating-related deformation associated with development of a subduction complex in the Late Ordovician at the eastern extremity of the Lachlan Fold Belt.

In this account we report the results of a $^{40}Ar/^{39}Ar$ and K–Ar study of samples from the south coast of New South Wales (Figure 1). We have found that the $^{40}Ar/^{39}Ar$ data are influenced by inherited mica that was not recrystallised during metamorphism associated with deformation, as well

*A fuller version of Table 1 is a Supplementary Paper lodged with the National Library of Australia (Manuscript Section); copies may be obtained from the Business Manager, Geological Society of Australia.

†Corresponding author: Chris_Fergusson@uow.edu.au

as recoil loss/redistribution of ^{39}Ar (Reuter & Dallmeyer 1989). Thus ^{40}Ar/^{39}Ar ages from low-grade pelites cannot be assumed to necessarily reflect a precise timing of metamorphic mica growth as has been commonly assumed (Foster *et al.* 1998, 1999).

PROBLEMS ASSOCIATED WITH ^{40}Ar/^{39}Ar DATING OF LOW-GRADE SLATES

Slates are attractive targets for ^{40}Ar/^{39}Ar geochronology, as they contain abundant white mica that crystallises at or below the closure temperature for argon diffusion—consequently, these phases have the potential to yield the time of peak metamorphism and/or deformation/tectonism, provided that these processes were relatively short lived. However, in reality, there are limitations to the technique (Reuter & Dallmeyer 1989) and new insights have emerged from vacuum encapsulation studies (Dong *et al.* 1995, 1997). Given these new developments and the importance of ^{40}Ar/^{39}Ar data to models for the formation of the Lachlan Fold Belt, an overview of the subject is presented below.

Inherited material

In addition to white micas formed during the deformation/metamorphic event to be dated, low-grade pelites may also contain inherited potassic phases that result in older apparent ages than the event being dated. In a classic study, Hunziker *et al.* (1986) traced the transformation of illite to muscovite across a transect from diagenetic grade to greenschist facies conditions and reported decreasing K–Ar ages with increasing metamorphic grade. Older K–Ar ages were attributed to the presence of detrital illite and complete rejuvenation of the K–Ar system was only achieved at the uppermost anchizone to epizone metamorphic transition and temperatures of 260 ± 30°C (Hunziker *et al.* 1986). On the basis of these and subsequent studies, Reuter and Dallmeyer (1989) concluded that white micas that crystallised under upper anchizone, or higher, metamorphic grades may be dated by K–Ar methods. For lower grade pelites, constraints on the age of the authigenic white mica population may be achieved by undertaking K–Ar analyses on successively smaller size fractions (<0.2–20 μm), a method known as illite age analysis (Pevear 1992).

Although usually dominated by fine-grained clay fractions, most pelitic rocks are heterogeneous and may also contain coarser detrital material, such as muscovite and feldspar grains (Reuter & Dallmeyer 1989). These grains may be incompletely reset during metamorphism, even under greenschist facies conditions (Dunlap 1997). The influence of detrital components will depend on their respective ages, relative abundance and argon-release behaviour. In the context of the present study, both Turner

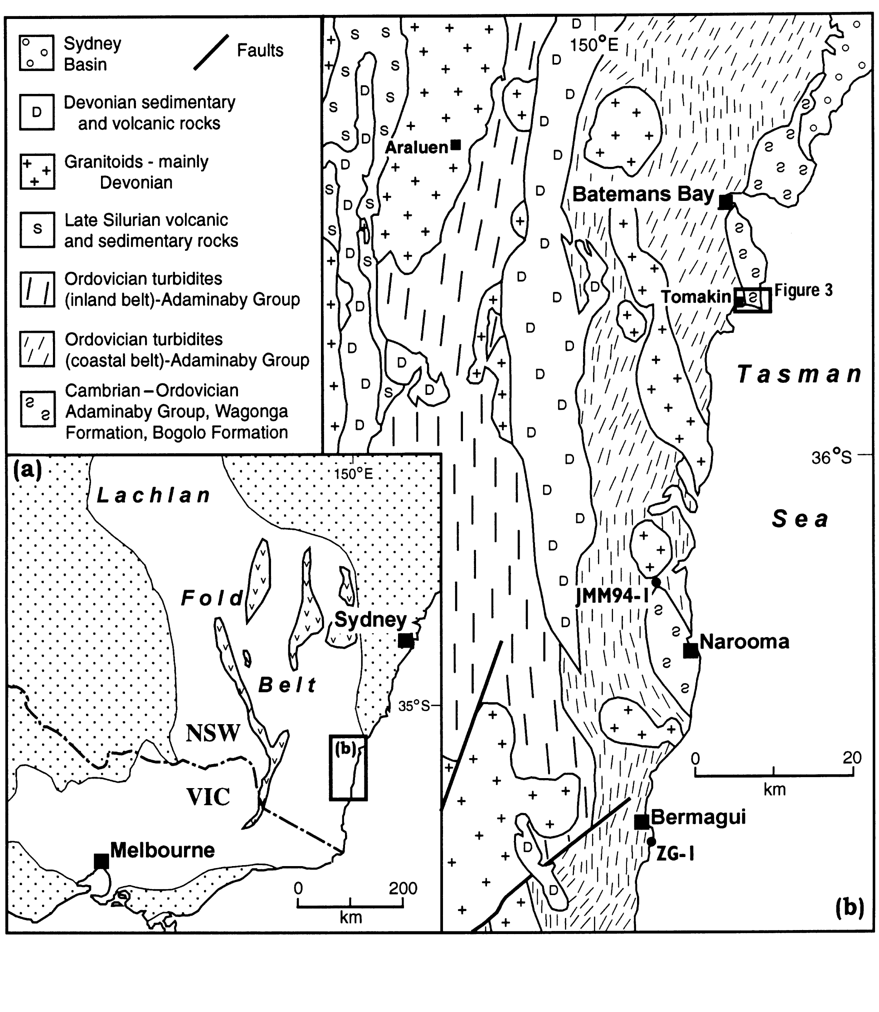

Figure 1 (a) Map of southeastern Australia showing the distribution of Ordovician island-arc rocks (v pattern) in the Lachlan Fold Belt and location of (b). Coarse stipple pattern, mainly Permian and younger sediments. (b) South coast of New South Wales between Batemans Bay and Bermagui with locations referred to in text and location of Figure 3. Subduction complex rocks coeval with island arc in (a) have been interpreted to include rocks at Batemans Bay, Narooma (the Narooma Anticlinorium) and the coastal belt Ordovician turbidites (after Powell 1983; Lewis *et al.* 1994; Miller & Gray 1996, 1997). JMM94-1 and ZG-1, ^{40}Ar/^{39}Ar age sample localities of Offler *et al.* (1998).

et al. (1996) and Foster *et al.* (1998) have reported $^{40}Ar/^{39}Ar$ ages ranging from 570 to 480 Ma for detrital muscovite grains in various sequences in the Lachlan Fold Belt.

Recoil loss/redistribution of ^{39}Ar

The $^{40}Ar/^{39}Ar$ method relies on the production of ^{39}Ar from ^{39}K during irradiation in a nuclear reactor (McDougall & Harrison 1999). As a consequence of the $^{39}K(n, p)^{39}Ar$ reaction, ^{39}Ar nuclei recoil variable distances according to their recoil energies (Turner & Cadogan 1974). As a result of this process, a portion of the ^{39}Ar produced during the irradiation procedure will be lost from grain margins. While the effects on large grains will be negligible, recoil ^{39}Ar losses from fine-grained, clay-size particles may be significant, resulting in anomalously old apparent ages (Reuter & Dallmeyer 1989). Investigations by Reuter and Dallmeyer (1989) and Dong *et al.* (1995, 1997) have suggested that the degree of ^{39}Ar loss is related to the grainsize, edge morphology and surface/volume ratios of relevant clay minerals. Dong *et al.* (1995) reported a strong correlation between illite crystallinity and the fraction of ^{39}Ar recoil loss (Figure 2). They attributed this to the fact that illite crystallinity is related to illite packet size, which is a function of the proportion of dislocations, voids and layer terminations. In other words, the formation of densely packed illite packets (low illite crystallinity values) reduces the effective surface/volume ratio and inhibits the loss of ^{39}Ar through reimplantation into adjacent illite lamellae. The effects of recoil loss of ^{39}Ar can be assessed either by comparison of K–Ar and total-gas $^{40}Ar/^{39}Ar$ ages or by vacuum encapsulation $^{40}Ar/^{39}Ar$ experiments (Dong *et al.* 1995, 1997).

In addition to recoil loss, ^{39}Ar nuclei may also recoil into adjacent grains of other minerals (Reuter & Dallmeyer 1989). In the case of slates, these minerals will generally be potassium-poor and may include quartz, chlorite and albite. As a consequence of this process, argon released from the latter phases may yield anomalously young apparent ages due to a decrease in their $^{40}Ar^{*}/^{39}Ar$ ratio ($^{40}Ar^{*}$ is radiogenic argon). As these phases may release argon at different temperatures to the degassing of white micas, recoil redistribution of ^{39}Ar can produce markedly discordant $^{40}Ar/^{39}Ar$ spectra (Lo & Onstott 1989; Reuter & Dallmeyer 1989).

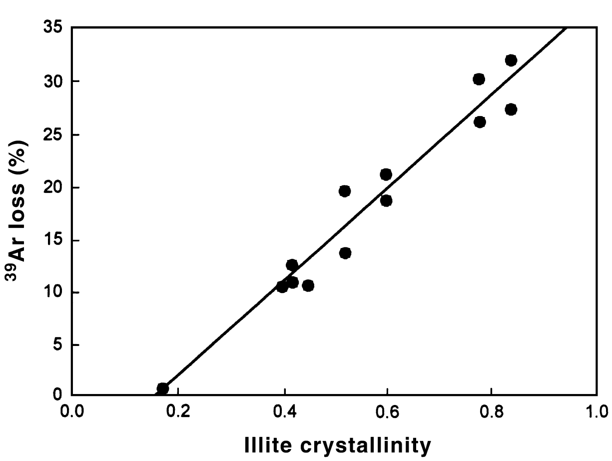

Figure 2 Correlation between illite crystallinity and ^{39}Ar loss (after Dong *et al.* 1995 figure 3). Illite crystallinity values are calculated from the half-height peak widths of illite peaks, determined from X-ray diffraction (XRD) patterns of treated samples and standards (Kisch 1991).

Extraneous argon

During mineral crystallisation or thermal rejuvenation, potassic phases such as white micas may incorporate argon with a non-atmospheric composition. Anomalously old ages recorded for phengites from high-pressure metamorphic rocks in the Alps have been attributed to the incorporation of excess argon from argon-rich metamorphic fluids (Arnaud & Kelley 1995). Although cases of contamination by excess argon in low-temperature slate and phyllite are rare, Leitch and McDougall (1979) reported a correlation between K–Ar ages and the degree of late-stage deformation for slate and phyllite from the Nambucca Slate Belt, New South Wales. The implication of this study is that reactivation or overprinting of existing structures may release fluids from older buried rocks that have elevated $^{40}Ar/^{39}Ar$ ratios, leading to anomalously old apparent ages.

$^{40}Ar/^{39}Ar$ step-heating spectra

Recent studies have demonstrated that *in vacuo* heating of hydrous phases yields apparent age spectra that do not reproduce the actual argon distributions in mineral grains (Phillips & Onstott 1989; Lee *et al.* 1991; Phillips 1991; Sletten & Onstott 1998). These and other studies have demonstrated that hydrous minerals do not release their argon by volume diffusion (Gaber *et al.* 1988). Instead these minerals (including illite) undergo dehydroxylation and delamination during vacuum heating, resulting in extensive homogenisation of internal argon concentration gradients (Onstott *et al.* 1997). For this reason, Lo *et al.* (2000) have suggested that step-heating analyses of pure biotite grains should always yield plateau age spectra, regardless of their internal argon concentrations. In other words, the achievement of a plateau age for hydrous minerals is not a guarantee that the age is accurate or geologically meaningful, as is generally considered. Lo *et al.* (2000) concluded that discordant age spectra from hydrous phases are likely to reflect the presence of additional phases, age populations and/or recoil loss/redistribution effects.

Many metapelites from the Lachlan Fold Belt have been subjected to step-heating analyses using a defocused laser beam (Offler *et al.* 1998; Foster *et al.* 1999). During laser heating, the laser beam impinges on the top of the sample. In addition, the laser energy is not absorbed uniformly by most materials. Consequently, laser heating may produce large temperature gradients, resulting in further homogenisation of step-heating release spectra and the achievement of apparent plateau ages that may have little geological significance.

Implications for the current study

The interpretation of $^{40}Ar/^{39}Ar$ step-heating data obtained from whole-rock slates is dependent on an accurate assessment of the limitations outlined above. To determine the effects of coarse detrital components, slate samples with variable abundance of detrital muscovite were analysed in the present study. To assess the effects of recoil loss of ^{39}Ar, the ^{40}Ar/^{39}Ar step-heating results are compared with K–Ar analyses conducted on whole-rock chips from the same crush fractions.

GEOLOGICAL BACKGROUND

In the Batemans Bay and Narooma districts, the Lachlan Fold Belt is dominated by three units: (i) the Adaminaby Group, comprising Ordovician quartz turbidites; (ii) the Wagonga Formation, with chert, black mudstone and mafic volcanics; and (iii) tectonic mélange of the Bogolo Formation (Jenkins *et al.* 1982; Powell 1983; Lewis *et al.* 1994). The Bogolo Formation is a mixture of the Adaminaby Group and the Wagonga Formation (C. L. Fergusson & P. Frikken unpubl. data). These rock units have been interpreted as an east-facing subduction complex related to a west-dipping Ordovician subduction zone (Jenkins *et al.* 1982; Powell 1983, 1984; Bischoff & Prendergast 1987).

In the Batemans Bay district the Wagonga Formation contains late Darriwilian to earliest Gisbornian conodonts in chert (Figure 3) (I. R. Stewart *in* Frikken 1997; Stewart & Glen 1991) and late Eastonian and early Bolindian graptolites (Jenkins *et al.* 1982); whereas in the Narooma region it contains several conodont assemblages that indicate a Late Cambrian to Late Ordovician age (Stewart & Glen 1991). Middle to Late Cambrian fossils occur in limestone clasts and beds associated with mafic volcanic breccias at Burrewarra Point (Bischoff & Prendergast 1987). At Melville Point conodonts recovered from chert of the Wagonga Formation and the overlying basal Adaminaby Group are of latest Cambrian to earliest Ordovician age (Bischoff & Prendergast 1987).

Powell (1983, 1984; modified by Powell & Rickard 1985) developed a structural history for the south coast involving four regional deformations.

The first regional folding event is widely developed and formed north-trending upright, tight to isoclinal folds, which Powell (1983) related to an end-Silurian event that post-dated deposition of Upper Silurian limestone 50 km southwest of Batemans Bay and pre-dated intrusion of plutons of the Lower Devonian Bega Batholith. This deformation involved development of an early slaty cleavage in Ordovician turbidites (S* of Powell & Rickard 1985).

A second regional folding event has been related by Powell (1983) to the formation of a regional conjugate set of strike-slip faults with sinistral northwest-trending structures and dextral northeast-trending structures. Displacements along these faults were thought to have occurred in the mid-Devonian as they offset plutons of the Bega Batholith and volcanic rocks of the mid-Devonian Boyd Volcanic Complex, but pre-date the Upper Devonian Merrimbula Group (Powell 1983).

A third regional folding event has affected Upper Devonian rocks in the region and is part of a Carboniferous deformation that is widespread throughout the Lachlan Fold Belt. North-trending upright folds and associated steeply dipping faults formed during this event (Powell 1984).

The fourth and last significant deformation formed kinks and kink-like folds that are developed at different scales throughout the region and include the megakinks of Powell *et al.* (1985).

Miller and Gray (1996, 1997) described tectonic mélanges of the Bogolo Formation, bedding-parallel cleavage, inferred bedding-parallel contractional duplication of the Ordovician turbidite succession, tight to isoclinal recumbent folding in the turbidite succession, and tight folds in cherts of the Wagonga Formation. They related these features to ongoing underplating-related deformation at

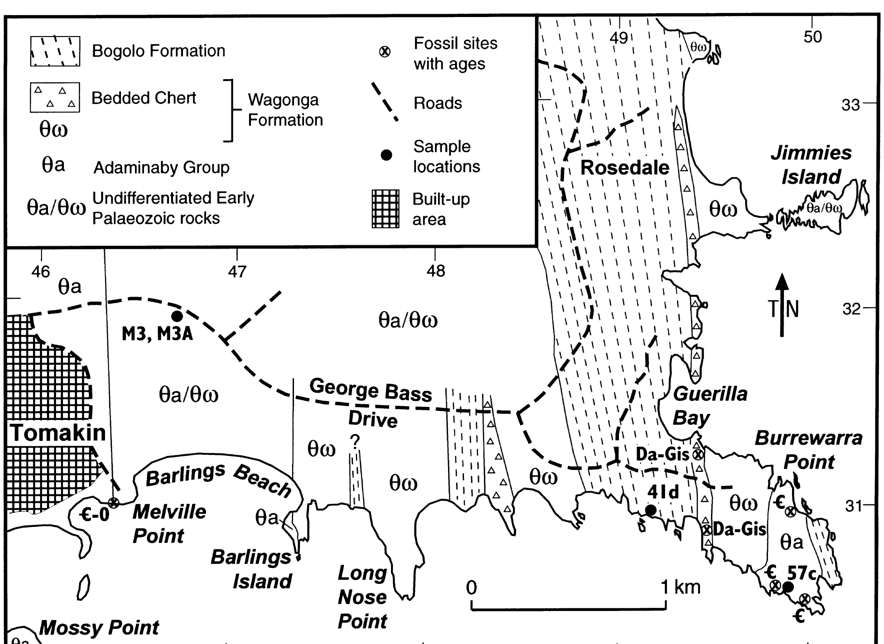

Figure 3 Map of sample locations along the coastline south of Batemans Bay (Tomakin–Burrewarra Point area). Geology after unpublished mapping of C. L. Fergusson and P. Frikken. Note that Cambrian limestones documented by Bischoff and Prendergast (1987) occur associated with basaltic breccia amongst the eastern zone of the Adaminaby Group at Burrewarra Point. Grid from the Mogo 1:25 000 map sheet. Cenozoic sediments not depicted. Locations of Cambrian (Burrewarra Point), latest Cambrian – earliest Ordovician (Melville Point) and Darriwilian–Gisbornian (Guerilla Bay, west of Burrewarra Point) are marked (from Bischoff & Prendergast 1987; Stewart & Glen 1991; Frikken 1997).

the base of the evolving subduction complex. Offler *et al.* (1998) reported the results of two $^{40}Ar/^{39}Ar$ plateau whole-rock ages on Ordovician slate, at least one of which contains an early slaty cleavage (the S* of Powell & Rickard 1985). They interpreted these ages [sample ZG-1 (445 ± 2 Ma); sample JMM94-1 (450 ± 3 Ma)] as indicating mica crystallisation (i.e. the time of formation of S*) and therefore indicated a latest Ordovician age for the underplating event. The younger age (sample ZG-1) is considered by Offler *et al.* (1998) to be the more reliable of the two ages. Offler *et al.* (1998) suggested that metamorphic temperatures in the eastern Lachlan Fold Belt were in the region of 250–300°C, based on mid to upper anchizonal conditions and dynamic recrystallisation of quartz.

Detailed mapping of the headlands between Batemans Bay and Tomakin has established that an intense moderately to steeply west-dipping S_2 cleavage, axial planar to abundant close to isoclinal folds affects most rocks (Powell 1983; C. L. Fergusson & P. Frikken unpubl. data). These structures are regarded as part of Powell's (1983, 1984) first regional folding event. They overprint east–west-trending folds that contain no axial planar structure.

SAMPLE LOCATIONS AND DESCRIPTIONS

Four samples of slate have been selected for $^{40}Ar/^{39}Ar$ and K–Ar analyses. Two samples are from the southern side of Burrewarra Point (41d, 57c) and two from a road cutting along George Bass Drive, 1 km east of Tomakin (M3, M3A, Figure 3). Three of the samples are from cleaved units (57c, M3, M3A) in the Adaminaby Group whereas the other sample is from highly cleaved matrix of the tectonic mélange of the Bogolo Formation.

Sample 41d (Mogo 1:25 000 sheet, 249200 6030925) is a highly fissile slate with a continuous white mica fabric that encloses lenticular siltstone fragments (Figure 4a). Fragments readily break off the sample and are as small as a millimetre or less in length. Microscopically they are bounded by fine veinlets (fractures?) cutting obliquely at a low angle to the main cleavage. The cleavage and fissility dip at 50–70° to the west throughout the outcrop.

Sample 57c (Mogo 1:25 000 sheet, 249910 6030530) comes from a slate intercalated amongst disrupted quartz turbidites (tectonic mélange) of the Adaminaby Group and nearby are pods and lenticles of highly vesicular greenstone (including one of the three Cambrian limestone localities documented by Bischoff and Prendergast 1987). This sample contains a single well-defined mica fabric (Figure 4b). The cleavage is also dipping to the west at 50–60°.

Samples M3 and M3A (Mogo 1:25 000 sheet, 246700 6031950) are both from the same road cutting in Adaminaby Group turbidites that contain the regional cleavage dipping at 50° to the west. Sample M3A contains a spaced dissolution-style cleavage (Figure 4c) whereas M3 has a

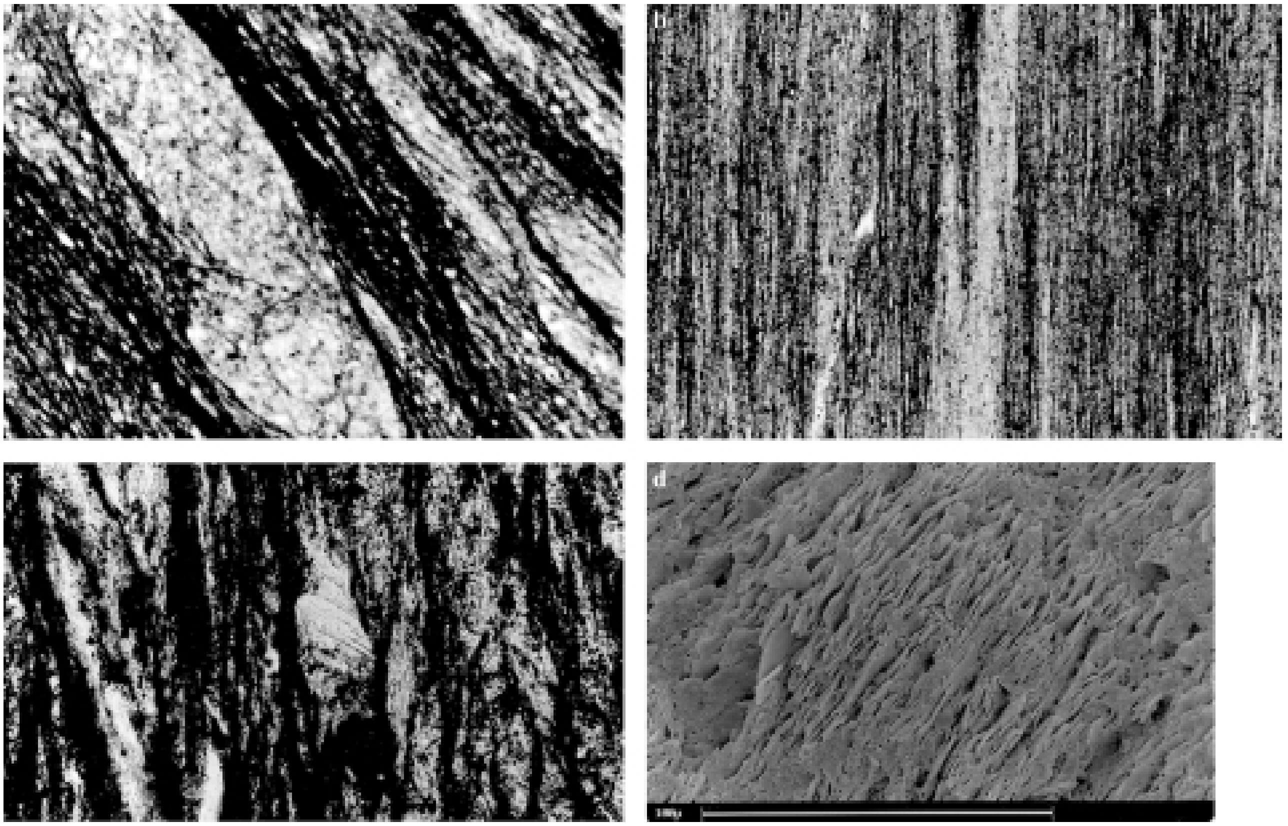

Figure 4 Photomicrographs showing microstructure of the four $^{40}Ar/^{39}Ar$ and K–Ar whole-rock samples. (a) Sample 41d: scaly slaty cleavage enclosing lenticular fragments of siltstone (~1.5 mm width). (b) Sample 57c: continuous cleavage in slate (~1.5 mm width). (c) Sample M3A: well-developed bedding-parallel cleavage with detrital muscovite flakes locally oblique to cleavage (~0.6 mm width). (d) SEM photograph of Sample M3: well-developed mica fabric cut by a spaced cleavage (bar scale 100 μm).

well-developed mica fabric (Figure 4d). M3 also contains a crenulation cleavage at a low angle to the slaty cleavage. M3 is a finer grained rock than M3A, which includes siltstone and fine sandstone layers and contains larger flakes of muscovite that are locally oblique to the cleavage, but more typically are at a low angle to or subparallel to the cleavage. These muscovite flakes are kinked and strained, indicating that they pre-date the cleavage in M3A and are detrital in origin.

X-ray diffraction (XRD) analyses (carried out by T. Eggleton, Department of Geology, Australian National University) indicate that all four samples are dominated by white mica, chlorite and quartz. Small quantities of albite may be present in sample 51C, while samples M3 and M3A contain vermiculite interlayered with chlorite. Illite crystallinity (IC) values were not determined for the current samples, although previous work in the Batemans Bay area yielded IC values ranging from 0.27 to 0.32 (Offler *et al.* 1998).

Table 1 Representative $^{40}Ar/^{39}Ar$ analytical data for Batemans Bay slate and muscovite samples.

Temp °C	Cum ^{39}Ar	Vol ^{39}Ar $\times 10^{-14}$ mol	$^{40}Ar/^{39}Ar$	$^{37}Ar/^{39}Ar$	$^{36}Ar/^{39}Ar$	$^{40}Ar^*$ (%)	$^{40}Ar^*/^{39}Ar$	Age ± 1σ (Ma)
41d Slate; 0.50 mg; J-value = 0.008449 ± 0.000034								
500	0.0207	0.329	19.250	0.1383	0.0179	72.38	13.934	200.8 ±2.6
600	0.1244	1.654	19.223	0.0197	0.0025	95.91	18.437	261.2 ±1
650	0.1645	0.638	30.103	0.0024	0.0018	98.10	29.532	401.9 ±3.8
700	0.5511	6.162	34.988	0.0001	0.0007	99.29	34.739	464.3 ±3.5
725	0.6973	2.330	33.411	0.0007	0.0008	99.11	33.113	445.0 ±3.5
750	0.7897	1.474	32.557	0.0010	0.0012	98.81	32.168	433.8 ±2.3
775	0.8460	0.898	32.520	0.0004	0.0017	98.32	31.400	424.5 ±2.1
800	0.8840	0.605	32.877	0.0026	0.0016	98.44	32.366	436.1 ±3
825	0.9115	0.438	34.109	0.0324	0.0031	97.17	33.143	445.4 ±2
850	0.9297	0.290	36.136	0.0053	0.0035	96.97	35.039	467.8 ±3.4
875	0.9476	0.286	37.185	0.0054	0.0052	95.77	35.613	474.6 ±2.7
900	0.9643	0.268	37.270	0.0058	0.0041	96.58	35.997	479.1 ±2
950	0.9841	0.315	38.059	0.0646	0.0043	96.56	36.753	487.9 ±3.1
1000	0.9939	0.155	36.460	0.2184	0.0116	90.55	33.021	443.9 ±6.1
1100	0.9968	0.046	48.562	0.1001	0.0622	62.07	30.143	409.3 ±20
1350	1.0000	0.051	90.626	0.0659	0.2488	18.82	17.053	242.8 ±32.5
57c Slate; 0.47 mg; J-value = 0.008386 ± 0.000034								
500	0.0233	0.197	16.378	0.0795	0.0264	52.06	8.526	124.6 ±2.2
600	0.0838	0.550	25.808	0.0199	0.0048	94.33	24.345	335.3 ±1.5
650	0.1705	0.694	34.437	0.0013	0.0037	96.70	33.300	444.5 ±2.7
700	0.3032	1.121	34.545	0.0015	0.0024	97.77	33.774	450.1 ±1.7
725	0.4140	0.936	34.143	0.0153	0.0028	97.48	33.283	444.3 ±1.3
750	0.5231	0.922	33.283	0.0019	0.0022	97.90	32.583	436.0 ±1.6
775	0.5678	0.378	32.893	0.0025	0.0038	96.43	31.719	425.7 ±1.8
800	0.6475	0.674	32.293	0.0220	0.0021	97.96	31.634	424.7 ±3.1
825	0.7225	0.633	32.573	0.0015	0.0026	97.45	31.743	426.0 ±1.4
850	0.7921	0.589	32.870	0.0060	0.0034	96.82	31.824	426.9 ±2.2
875	0.8482	0.474	33.731	0.0143	0.0037	96.66	32.605	436.2 ±1.7
900	0.9094	0.518	33.304	0.0018	0.0038	96.50	32.140	430.7 ±3.3
950	0.9774	0.574	33.760	0.0016	0.0042	96.20	32.478	434.7 ±2.1
1000	0.9920	0.123	41.307	0.0076	0.0208	85.01	35.116	465.8 ±4.4
1100	0.9974	0.046	52.266	1.0721	0.0595	66.51	34.788	462.0 ±10.5
1200	1.0000	0.021	62.951	0.1011	0.1251	41.22	25.953	355.4 ±17.2
M3A Slate; 0.57 mg; J-value = 0.008411 ± 0.000025								
500	0.0100	0.103	14.750	0.0759	0.0110	77.66	11.456	166.0 ±3.4
600	0.0884	0.808	20.786	0.0299	0.0055	91.96	19.115	269.0 ±2.2
650	0.1977	1.128	33.923	0.0016	0.0029	97.32	33.013	442.1 ±1.2
675	0.2874	0.924	36.760	0.0011	0.0021	98.21	36.103	478.4 ±1.5
700	0.3904	1.062	36.652	0.0010	0.0019	98.35	36.046	477.7 ±3.5
725	0.5091	1.224	36.187	0.0008	0.0018	98.37	35.596	472.5 ±1.4
750	0.6392	1.341	35.503	0.0008	0.0020	98.22	34.872	464.0 ±2.1
775	0.7398	1.037	35.212	0.0010	0.0015	98.63	34.730	462.3 ±1.6
800	0.8002	0.623	35.234	0.0016	0.0017	98.44	34.684	461.8 ±3.7
825	0.8475	0.487	35.948	0.0041	0.0029	97.48	35.040	466.0 ±1.3
850	0.8856	0.393	36.328	0.0026	0.0036	96.91	35.206	467.9 ±4.7
875	0.9136	0.289	38.010	0.0035	0.0032	97.35	37.004	488.9 ±3.6
900	0.9384	0.255	38.717	0.0040	0.0043	96.59	37.396	493.4 ±2.4
950	0.9703	0.329	39.851	0.0124	0.0040	96.92	38.623	507.5 ±2.4
1000	0.9880	0.183	42.014	0.1257	0.0066	95.25	40.022	523.5 ±4.8
1100	0.9977	0.100	44.356	0.0101	0.0128	91.39	40.538	529.3 ±6.6
1350	1.0000	0.024	111.31	0.4438	0.2752	26.95	30.002	406.0 ±33.1

ANALYTICAL TECHNIQUES

Whole-rock samples from the four Batemans Bay localities were crushed by hand, sieved and washed. Approximately 200 mg of each sample, comprising 0.5–1.0 mm chips, was hand picked, avoiding altered and/or iron-stained fragments. In addition, a muscovite separate (180–200 μm) was prepared from sample M3A using conventional magnetic and heavy-liquid separation methods. Final hand picking of the muscovite ensured a purity of >99%. $^{40}Ar/^{39}Ar$ and K–Ar analyses were carried out at the Research School of Earth Sciences, Australian National University. Conventional K–Ar analytical techniques were similar to those described by McDougall (1985).

The $^{40}Ar/^{39}Ar$ dating technique is described in detail by McDougall and Harrison (1999). Approximately 5 mg of each sample was irradiated in a cadmium-lined aluminium irradiation canister together with interspersed aliquots of the flux monitor GA1550 (Age = 97.9 Ma: McDougall & Roksandic 1974). [Note that recent results obtained by Renne *et al.* (1998) indicate an age of 98.8 ± 1.0 Ma for GA1550 biotite: for the purpose of comparisons with previous data from the Lachlan Fold Belt the earlier date of 97.9 Ma is utilised in the current study.] ^{40}Ar production from potassium was determined from analyses of degassed potassium glass. The irradiation canister was irradiated for 504 hours in position X33 or X34 of the ANSTO, HIFAR reactor, Lucas Heights. The canister was inverted three times during the irradiation, which reduced neutron flux gradients to <2% along the length of the canister. After irradiation, 0.3–1.0 mg aliquots of each sample were loaded into tin-foil packets for analysis and step-heated in a tantalum resistance furnace. $^{40}Ar/^{39}Ar$ step-heating analyses were carried out on a VG MM12 mass spectrometer using an electron multiplier detector. Sensitivity was approximately 7×10^{-17} mol/mv. Mass

Table 1 (cont.)

Temp °C	Cum ^{39}Ar	Vol ^{39}Ar $\times 10^{-14}$ mol	$^{40}Ar/^{39}Ar$	$^{37}Ar/^{39}Ar$	$^{36}Ar/^{39}Ar$	$^{40}Ar^*$ (%)	$^{40}Ar^*/^{39}Ar$	Age ± 1σ (Ma)
M3A Muscovite; 0.49 mg; J-value = 0.0026280 ± 0.0000079								
500	0.0058	0.059	50.556	0.1014	0.0495	71.01	35.90	162.7 ±1.6
600	0.0212	0.158	95.458	0.0162	0.0213	93.37	89.13	379.7 ±2.6
650	0.0386	0.178	121.08	0.0053	0.0126	96.88	117.31	484.8 ±1.6
700	0.0668	0.288	122.19	0.0033	0.0090	95.41	119.48	492.6 ±2.5
725	0.0917	0.255	123.81	0.0037	0.0098	97.64	120.88	497.7 ±2.6
750	0.1197	0.287	124.72	0.0033	0.0078	98.13	122.39	503.1 ±2.7
775	0.1539	0.351	123.73	0.0027	0.0066	98.40	121.75	500.8 ±1.8
800	0.1957	0.428	124.23	0.0022	0.0053	98.70	122.62	503.9 ±2.2
825	0.2493	0.549	124.50	0.0017	0.0049	98.81	123.50	507.1 ±3.2
850	0.3204	0.728	125.49	0.0013	0.0041	98.99	124.23	509.7 ±2.7
875	0.4058	0.875	124.70	0.0011	0.0036	99.11	123.59	507.4 ±1.9
900	0.5261	1.232	124.39	0.0008	0.0028	99.30	123.52	507.1 ±4.6
925	0.5995	0.752	126.53	0.0026	0.0033	99.19	125.50	514.2 ±3.7
950	0.6748	0.771	126.90	0.0013	0.0039	99.06	125.71	515.0 ±1.2
975	0.7344	0.610	125.75	0.0016	0.0045	98.91	124.60	511.0 ±1.3
1000	0.7833	0.502	128.04	0.0019	0.0055	98.71	126.39	517.4 ±4.3
1050	0.8716	0.904	127.42	0.0011	0.0046	98.91	126.03	516.1 ±3.2
1100	0.9765	1.075	128.95	0.0009	0.0043	98.98	127.63	521.8 ±3
1150	0.9969	0.209	129.32	0.0046	0.0129	97.01	125.46	514.1 ±2.6
1350	1.0000	0.032	154.56	0.0307	0.1846	64.68	99.97	420.8 ±8.9
M3 Slate; 0.49 mg; J-value = 0.008443 ± 0.000025								
500	0.0322	0.599	12.447	0.0516	0.0064	84.42	10.508	153.3 ±1.7
600	0.1585	2.348	26.897	0.0025	0.0032	96.34	25.914	356.8 ±2.1
650	0.3138	2.889	35.370	0.0007	0.0011	98.96	35.002	467.0 ±2.8
700	0.5046	3.548	36.398	0.0003	0.0009	99.11	36.075	479.5 ±1.8
725	0.6595	2.880	36.078	0.0003	0.0011	99.00	35.717	475.4 ±2.1
750	0.7598	1.864	35.953	0.0005	0.0012	98.89	35.555	473.5 ±2.1
775	0.8406	1.504	35.848	0.0007	0.0010	99.02	35.495	472.8 ±3.1
800	0.8965	1.039	36.833	0.0009	0.0015	98.66	36.339	482.6 ±2.9
825	0.9309	0.640	37.155	0.0015	0.0025	97.90	36.374	483.0 ±4.9
850	0.9524	0.400	38.348	0.0024	0.0029	97.64	37.443	495.4 ±3.6
875	0.9702	0.331	39.054	0.0036	0.0039	96.91	37.846	500.1 ±4.8
900	0.9814	0.208	39.438	0.0047	0.0045	96.49	38.053	502.5 ±3.8
950	0.9930	0.217	39.767	0.0045	0.0047	96.37	38.323	505.6 ±1.5
1000	0.9975	0.082	42.368	0.0170	0.0169	88.12	37.336	494.2 ±5.1
1100	0.9990	0.028	49.194	0.0357	0.0393	76.29	37.533	496.5 ±26.9
1350	1.0000	0.020	104.790	0.0504	0.2458	30.65	32.123	432.8 ±70.6

Isotopic ratios are corrected for mass spectrometer backgrounds, mass discrimination and radioactive decay.
$^{40}Ar^*/^{40}Ar$, where $^{40}Ar^*$ is radiogenic argon.
Errors are 1σ uncertainties and exclude the error in the J-value.
Correction factors: $(^{36}Ar/^{37}Ar)_{Ca}$ = 3.5E-4; $(^{39}Ar/^{37}Ar)_{Ca}$ = 7.86E-4; $(^{40}Ar/^{39}Ar)_{K}$ = 0.040; $\lambda^{40}K$ = 5.543E-10y^{-1}.

discrimination was monitored by analyses of standard air volumes. Correction factors for interfering reactions are as follows: $(^{36}Ar/^{37}Ar)_{Ca}$ = 3.50 (±0.02) × 10^{-4}; $(^{39}Ar/^{37}Ar)_{Ca}$ = 7.9 (±0.5) × 10^{-4} (Tetley *et al.* 1980; McDougall & Harrison 1999); $(^{40}Ar/^{39}Ar)_K$ = 0.040 (±0.005). The reported data have been corrected for mass spectrometer backgrounds, mass discrimination and radioactive decay. Errors associated with the age determinations are 1σ uncertainties and exclude errors in the J-value estimates. The error on the J-value is ±0.35%, excluding the uncertainty in the age of GA1550 (~1%). Decay constants are those recommended in Steiger and Jäger (1977).

$^{40}Ar/^{39}Ar$ AND K–Ar RESULTS

Representative K–Ar and $^{40}Ar/^{39}Ar$ analytical results from the four slate samples are listed in Tables 1 and 2, respectively (the full dataset is available from the authors on request). All samples were analysed in duplicate to assess possible heterogeneities within individual samples. Apparent age spectra are presented in Figure 5. Age plateaus are defined as flat portions of age spectra consisting of at least three successive steps that comprise a significant proportion of the ^{39}Ar released, and have ages that are concordant at the 95% confidence level, based on internal errors.

Two analyses of detrital muscovite from sample M3A yielded similar age spectra, with apparent ages increasing from a minimum of 163 ± 2 Ma to plateau ages of 505 ± 3 Ma and 513 ± 3 Ma, respectively (Figure 5a). As these samples are composites of several detrital muscovite grains, probably with a range of ages, the 'plateau' results are considered to be average ages, of limited geological significance. Therefore, the discrepancy between the two 'plateau' ages is not unexpected and reflects the heterogeneity in the age population. These results are consistent with $^{40}Ar/^{39}Ar$ ages (570–480 Ma) for detrital muscovite in Ordovician sandstones of the Lachlan Fold Belt in eastern and western Victoria (Turner *et al.* 1996; Foster *et al.* 1998) and support the derivation of these rocks from the Adelaide Fold Belt (Fergusson & Tye 1999). More importantly, the results confirm that inheritance has not been eliminated from this sample by low-grade metamorphism.

The apparent age spectra of all the whole-rock slate samples exhibit very similar discordance patterns, with apparent ages increasing initially before decreasing to form a mid-temperature 'saddle', followed by a general increase in apparent ages at the highest temperature steps. This pattern is very typical of that obtained from many slates worldwide (Wright & Dallmeyer 1991), suggesting common causative processes. The young apparent ages associated with the lowest temperature steps are likely due to loss of argon in response to a younger thermal event and/or alteration/weathering affects. The main features of each of the current step-heating spectra are summarised in Table 3.

Step-heating analyses of slate fragments from sample M3A show apparent ages increasing from a minimum of

Table 2 K–Ar age data on whole-rock slate samples from Batemans Bay.

Sample no.	Sample type	K (wt%)	$^{40}Ar^*$ ($\times 10^{-9}$ mol/g)	$^{40}Ar^*$ (%)	Age ± 1σ (Ma)	Mean age ± 1σ (Ma)
41d(1)	Slate	3.30, 3.27	2.72	80.2	424 ± 5	423 ± 4
41d(2)		3.30, 3.27	2.72	98.1	423 ± 4	
57c(1)	Slate	2.42, 2.41	2.03	40.2	431 ± 5	409 ± 16
57c(2)		2.42, 2.42	1.85	57.4	402 ± 5	
57c(3)		2.42, 2.41	1.84	96.9	393 ± 4	
M3A(1)	Slate	3.04, 3.05	2.62	97.4	437 ± 5	438 ± 4
M3A(2)		3.04, 3.05	2.63	92.7	440 ± 4	
M3(1)	Slate	5.78, 5.82	4.95	84.5	435 ± 5	429 ± 6
M3(2)		5.78, 5.82	4.79	22.6	423 ± 6	

$\lambda^{40}_K = 5.543 \times 10^{-10}\ y^{-1}$; $^{40}K/K = 1.167 \times 10^{-4}$ mol/mol; $^{40}Ar^*$, radiogenic argon.

Table 3 Summary of $^{40}Ar/^{39}Ar$ age spectra results.

Sample no.	Sample type	Minimum age (Ma)	Maximum age (Ma)	Minimum 'saddle' age (Ma)	Total-gas age (Ma)	Plateau age (Ma)
41d(1)	Slate	234 ± 2	474 ± 2	424 ± 2	422 ± 2	–
41d(2)	Slate	201 ± 3	488 ± 3	425 ± 2	427 ± 3	–
57c(1)	Slate	66 ± 3	460 ± 8	419 ± 2	415 ± 2	–
57c(2)	Slate	125 ± 2	466 ± 4	425 ± 3	424 ± 2	–
M3(1)	Slate	293 ± 1	495 ± 2	470 ± 2	455 ± 2	–
M3(2)	Slate	153 ± 2	506 ± 2	473 ± 3	453 ± 3	–
M3A(1)	Slate	281 ± 2	546 ± 5	460 ± 2	455 ± 2	–
M3A(2)	Slate	166 ± 3	529 ± 7	462 ± 4	452 ± 2	–
M3A(3)	Muscovite	298 ± 4	508 ± 2	–	500 ± 3	505 ± 3
M3A(4)	Muscovite	163 ± 2	522 ± 3	–	506 ± 3	513 ± 3

166 ± 3 Ma at the lowest temperature, to a maximum of 546 ± 5 Ma (Figure 5b). The intermediate temperature steps exhibit a general saddle shape, with a minimum apparent age of 460 ± 2 Ma. As sample M3A contains significant amounts of (*ca* 500 Ma) detrital muscovite, the age spectra represent mixtures of inherited mica and new cleavage-forming metamorphic illite. The K–Ar whole-rock ages for this sample (437 ± 5 Ma; 440 ± 4 Ma) are some 15 million years younger than the total-gas integrated $^{40}Ar/^{39}Ar$ ages of 455 ± 2 Ma and 452 ± 2 Ma (Table 3). This result is consistent with recoil loss of a portion (~3.5%) of the ^{39}Ar from fine-grained white micas. Both recoil loss of ^{39}Ar and inheritance will lead to elevated apparent ages, thus providing only maximum age constraints for the cleavage-producing deformation.

$^{40}Ar/^{39}Ar$ spectra from sample M3 exhibit a minimum age of 153 ± 2 Ma, associated with a 500°C temperature increment, and a minimum 'within-saddle' age of 470 ± 2 Ma (Figure 5c). Total-gas integrated $^{40}Ar/^{39}Ar$ ages of 455 ± 2 Ma and 453 ± 3 Ma are distinctly older than associated K–Ar ages (435 ± 5 Ma; 423 ± 6 Ma). The clear implication is that sample M3 has also been affected by recoil loss

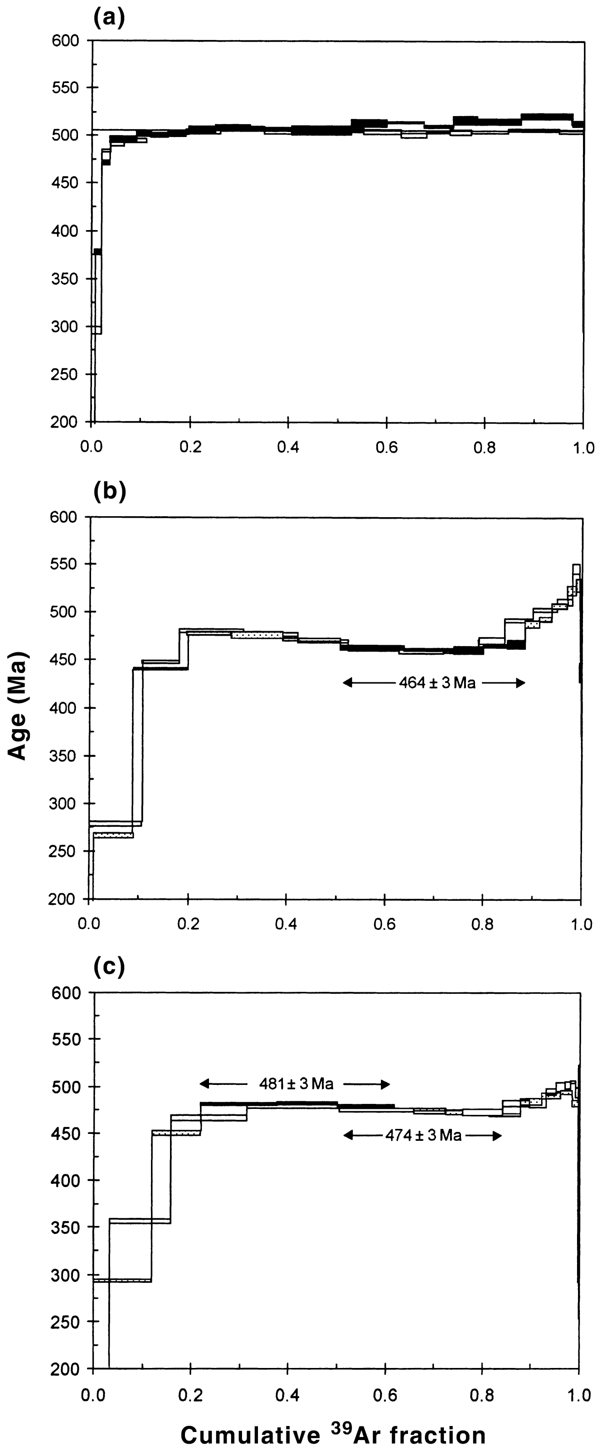

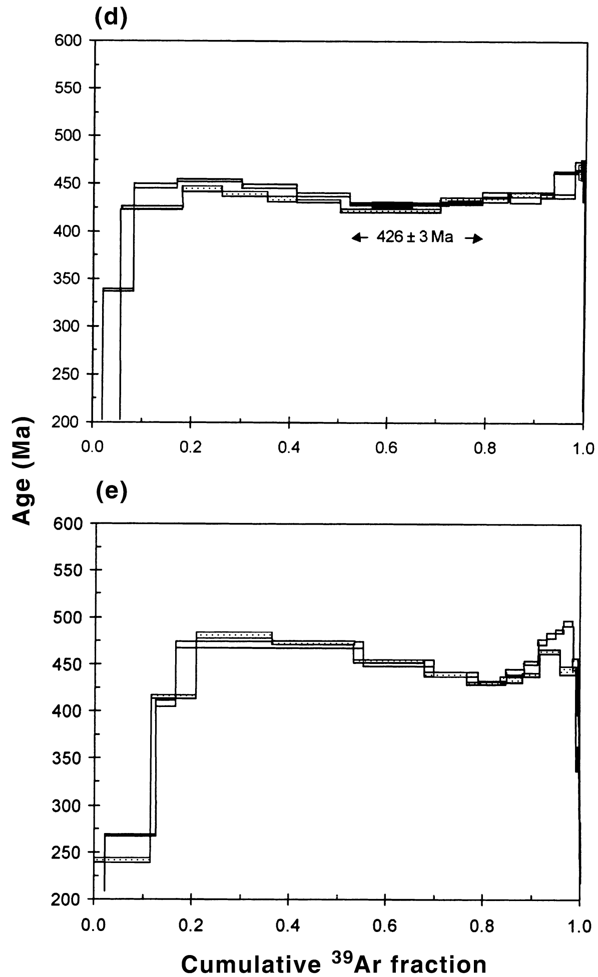

Figure 5 $^{40}Ar/^{39}Ar$ step-heating spectra for detrital muscovite and whole-rock slate chips from Batemans Bay samples. (a) M3A detrital muscovite samples with plateau ages of 505 ± 3 Ma (open symbols) and 513 ± 3 Ma (filled symbols). (b) Slate sample M3A. (c) Slate sample M3. (d) Slate sample 57c. (e) Slate sample 41d.

of ^{39}Ar (~4–7%) and by inheritance, even though detrital muscovite has not been detected in the thin-section of the sample (Figure 4c). Sample M3 is the only sample that has been affected by development of a crenulation cleavage. An alternative explanation relating to the uptake of excess ^{40}Ar is explored in the following section.

Sample 57c, an intensely cleaved slate, has $^{40}Ar/^{39}Ar$ total-gas ages of 415 ± 2 Ma and 424 ± 2 Ma, and K–Ar whole-rock ages of 429 ± 5 Ma, 402 ± 5 Ma and 393 ± 4 Ma (Figure 5d). It is unclear whether the oldest K–Ar age is due to sample heterogeneity or an analytical aberration. In the latter instance, the older $^{40}Ar/^{39}Ar$ ages would imply significant recoil loss of ^{39}Ar (~5%). If sample heterogeneity is a factor, recoil loss may be less important than with samples M3A and M3. In the latter case, the discordance associated with intermediate temperature steps (700–850°C) is probably due to recoil redistribution of ^{39}Ar.

Sample 41d, from a slaty tectonic mélange, exhibits $^{40}Ar/^{39}Ar$ integrated total-gas ages of 422 ± 2 Ma and 427 ± 3 Ma, and K–Ar whole-rock ages of 424 ± 5 Ma and 423 ± 4 Ma (Figure 5e). The general consistency of these results, accompanied by microscopic observations indicating few detrital mica grains (Figure 4a, b), suggest that in this sample ^{39}Ar recoil and inheritance problems may be of lesser importance. However, the age spectra are still discordant, with similar patterns to those from the other slate samples, suggesting some inheritance as well as significant recoil redistribution of ^{39}Ar into higher retentivity sites in the illite structure and/or adjacent phases such as chlorite and quartz.

$^{37}Ar_{Ca}/^{39}Ar_K$ ratios for all samples are listed in Table 1. Apart from small amounts of $^{37}Ar_{Ca}$ released at the lowest temperature steps, presumably from carbonates, $^{37}Ar_{Ca}$ contents are indistinguishable from blank levels for the majority of temperature increments. The apparent increase in $^{37}Ar_{Ca}/^{39}Ar_K$ ratios at the highest temperature steps (>900°C) is an artefact of decreasing ^{39}Ar levels rather than increasing ^{37}Ar contents. As the $^{37}Ar_{Ca}/^{39}Ar_K$ ratios do not influence the following discussions, Ca/K spectra have not been plotted.

DISCUSSION

Interpretation of $^{40}Ar/^{39}Ar$ data from whole-rock slate samples

Interpretation of $^{40}Ar/^{39}Ar$ step-heating data from whole-rock slate samples requires that all the potential problems of inheritance, recoil and extraneous argon are addressed. The analyses of detrital muscovite grains (180–250 μm) from sample M3A clearly indicate that deformation and metamorphism have not reset coarser white micas. As these grains are more retentive than fine-grained illite, step-heating analyses should differentiate between these components (Dong *et al.* 2000). To investigate this possibility, the argon release spectra for a detrital muscovite fraction is compared to that from sample 41d, which contains rare detrital muscovite, but abundant metamorphic illite (Figure 6). In this example, argon is released from fine-grained illite at much lower temperatures (500–750°C) than

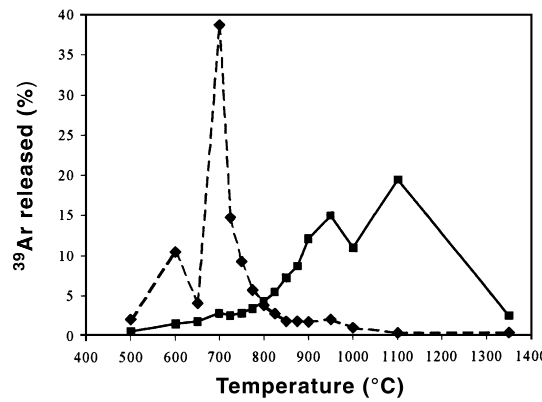

Figure 6 Argon release from detrital muscovite of sample M3A (■) compared with that from whole-rock slate chips of sample 41d (◆).

from detrital muscovite, which releases most (but not all) argon at temperatures above 800°C (Figure 6). Therefore, the highest temperature steps (>900°C) obtained from the slate samples are likely to be dominated by argon release from coarse-grained detrital white micas. Without exception, the Batemans Bay slate samples exhibit elevated apparent ages at the highest temperature increments, with the effects being least pronounced for samples 41d and 57c. However, this does not mean that the lower temperature increments are not affected by the presence of inherited material. Examination of the slate samples in thin-section indicates that many of the visible detrital muscovite grains have been disaggregated during the deformation process, producing a range of grainsizes. As grainsize is one of the controls on argon diffusion, disaggregation of detrital grains and the incorporation of detrital material with a range of grainsizes will result in a low temperature broadening of the temperature interval over which muscovite degasses. This might account for the elevated apparent ages recorded from most temperature steps of sample M3A, compared to ages from samples 41d and 57c.

The question of resetting of detrital clay fractions is more difficult to address with the current dataset. Reuter and Dallmeyer (1989) demonstrated that reliable K–Ar ages are only obtained once upper anchizone metamorphic conditions are reached (illite crystallinity indices are less than ~0.30). The current samples and most slates from the Lachlan Fold Belt exhibit illite crystallinity indices of ~0.30, suggesting that metamorphic conditions may have been close to the minimum temperatures required to completely reset detrital clay material. This question requires testing through K–Ar (or $^{40}Ar/^{39}Ar$ encapsulation) analyses of progressively finer clay fractions from selected samples and will be the subject of future work.

A number of studies of slates from the Lachlan Fold Belt have hinted at the possible effects of recoil loss/redistribution of ^{39}Ar (Foster *et al.* 1998; Offler *et al.* 1998). However, the manifestation and extent of the problem have not been evaluated. A simple comparison of K–Ar ages and $^{40}Ar/^{39}Ar$ total-gas ages has demonstrated that whole-rock slate samples from the current study are influenced by recoil loss of ^{39}Ar. Taking into account the uncertainties of both dating methods, it would appear that the quantities of ^{39}Ar lost during irradiation range from <2 to ~7%. These levels are similar to those reported for low-grade slates by Dong *et al.* (1995, 1997). This scenario is further complicated by the fact that recoil loss of ^{39}Ar is likely to be accompanied by recoil redistribution of ^{39}Ar from potassium-rich material into higher temperature retention sites within the illite structure and/or adjacent potassium-poor phases with different degassing patterns (Reuter & Dallmeyer 1989). If potassium-poor phases release argon over a different temperature range compared to the potassium-rich mineral, apparent ages associated with the potassium-poor material will be anomalously young. Dong *et al.* (1997) reported 'hump-shaped' $^{40}Ar/^{39}Ar$ spectra from K-bentonites and slates from the Welsh Basin, UK, which they suggested might be caused by recoil redistribution of ^{39}Ar. The combination of recoil loss and redistribution of ^{39}Ar almost certainly accounts for the decrease in apparent ages at intermediate temperature steps (700–800°C), which is then offset at higher temperatures by release from coarser detrital material.

Contamination by excess ^{40}Ar is relatively uncommon in low-grade pelites, presumably because deformation/metamorphism takes place in upper crustal environments dominated by meteoric fluids with atmospheric argon compositions. Nevertheless, Leitch and McDougall (1979) presented strong arguments for excess argon contamination in Nambucca slates that have undergone multiple episodes of deformation. Except for sample M3, the Batemans Bay slates are characterised by a single deformation fabric. Although sample M3 shows no signs of detrital components, it has experienced two deformation events and exhibits older apparent ages than the remaining samples. Therefore, one possible explanation might be the uptake of excess argon, released during the most recent deformation event. However, the later crenulation cleavage does not appear to be associated with substantial growth of new micas, suggesting low-temperature deformation and a reduced likelihood of excess argon contamination. The alternative explanation is that this sample contains detrital white mica that cannot be resolved in thin-section.

The above factors, coupled with the effects of dehydroxylation/delamination of hydrous phases during vacuum heating in the laboratory, place severe limitations on the interpretation of $^{40}Ar/^{39}Ar$ data from whole-rock slate samples. Inheritance, recoil loss of ^{39}Ar and extraneous ^{40}Ar all result in elevated apparent ages. Recoil redistribution of ^{39}Ar into low-potassium phases, coupled with variable degassing patterns, may produce anomalously young apparent ages in portions of the age spectra. Of the slate samples analysed in the current investigation, samples 41d and 57c appear to contain the lowest quantities of detrital muscovite. Although sample 41d may have lost minimal ^{39}Ar, the step-heating pattern is similar to the other samples, suggesting that recoil redistribution of ^{39}Ar is still a factor. It is likely that the maximum apparent ages associated with the lower temperature segments (700–800°C) of the age spectra will overestimate the time of cleavage formation due to recoil loss/redistribution effects. Sample 57c exhibits the youngest low temperature 'maximum' age of *ca* 440 Ma: therefore, the maximum age for cleavage formation is estimated at *ca* 440 Ma. At the same time, inheritance of coarse detritus and recoil effects are unlikely to have changed $^{40}Ar/^{39}Ar$ ratios by more than ~10%. Therefore, assuming that the clay fractions of samples 41d and 57c have been reset by the metamorphism/deformation, it is possible that cleavage formation occurred in the time interval 440–400 Ma.

Timing of regional deformation on the south coast of New South Wales

Our data only constrain the timing of regional deformation in the Batemans Bay district to <440 Ma. This is broadly consistent with the regional constraints listed by Powell (1983, 1984). He argued that the first set of north–south folds and axial-planar cleavage in the Ordovician rocks on the south coast of New South Wales could be mapped westwards into Upper Silurian strata in the Araluen district 50 km southwest of Batemans Bay (Figure 1). This has been confirmed by Wyborn and Owen (1986) who mapped the contact between the Upper Silurian and Ordovician successions and found only evidence of uplift and some tilting along the unconformity between them. They reported that the major deformation in the Araluen 1:100 000 map sheet area post-dated both successions. The north–south folds and related cleavage are cross-cut by intrusions of the Moruya and Bega Batholiths that have K–Ar cooling ages in the range 409–376 Ma and 379 Ma, respectively (Lewis *et al.* 1994). Therefore the deformation is constrained somewhere between 418 Ma (top of the Silurian: Tucker *et al.* 1998) and *ca* 409 Ma. In many areas geological constraints will be much broader than these, as Upper Silurian rocks are only found to the west, and most of the granitic plutons have few reliable published radiometric ages.

The new data from the Batemans Bay district require a reassessment of the $^{40}Ar/^{39}Ar$ ages of 450–445 Ma reported by Offler *et al.* (1998). Sample JMM94-1, from Narooma, is characterised by a highly discordant apparent age spectrum, which Offler *et al.* suspected had been affected by ^{39}Ar recoil. Sample ZG-1, from Bermagui, exhibits a much flatter age spectrum, with a reported plateau age of 445 ± 2 Ma. The latter sample is characterised by an IC value of ~0.24, which is unusually low for Lachlan Fold Belt slates (R. Offler pers. comm. 2000) and suggests minor recoil loss/redistribution effects. As with the Batemans Bay slates, the highest temperature steps of the Narooma/Bermagui samples have elevated apparent ages, suggesting the presence of minor quantities of detrital muscovite/feldspar. As inheritance and recoil produce elevated apparent ages, we would interpret the *ca* 445 Ma 'plateau' age as a maximum estimate for the time of deformation/metamorphism. However, as these effects are limited in the case of sample ZG-1, it is suggested that the age of metamorphism in the Bermagui area may be close to *ca* 440 Ma. If correct, then metamorphism at Narooma may pre-date deformation in the Batemans Bay region.

Implications for $^{40}Ar/^{39}Ar$ ages in the Lachlan Fold Belt

The lack of widespread stratigraphic constraints on regional deformation has been the main reason for the use of $^{40}Ar/^{39}Ar$ data to constrain the timing of deformation across the Lachlan Fold Belt (Foster *et al.* 1998, 1999). Significant proportions of these data have been obtained from whole-rock pelite samples. Stated and implied assumptions of these studies include complete replacement of diagenetic white micas by metamorphic micas, the absence or complete recrystallisation of inherited detrital material, and minimal ^{39}Ar recoil effects. Our data indicate that ^{39}Ar recoil and muscovite inheritance are likely to be common phenomena in the Lachlan Fold Belt. Therefore many $^{40}Ar/^{39}Ar$ whole-rock ages that presently exist on slates are more likely to indicate a broad upper constraint to the timing of deformation rather than a precise measurement of the timing of deformation (cf. Foster *et al.* 1998, 1999).

For example, Foster *et al.* (1999) analysed whole-rock slate samples from the central Lachlan Fold Belt and concluded that deformation commenced at *ca* 435 Ma in the northeast, and migrated to the southwest by *ca* 410 Ma. All samples are described as having 'plateau dates', some 'well-defined'. However, inspection of the age spectra (Foster *et al.* 1999 figure A1) reveals significant discordance in all spectra, with patterns broadly similar to those of the Batemans Bay samples (Figure 5). Clearly, the influences of inheritance and recoil loss/redistribution of ^{39}Ar require evaluation before the data can be interpreted correctly. Therefore, any conclusions regarding the migration of deformation fronts are likely to be premature.

The same rationale applies to $^{40}Ar/^{39}Ar$ whole-rock data from western Victoria. VandenBerg (1999) has regarded these ages as evidence for episodic deformation correlated with the Benambran Orogeny of the eastern Lachlan Fold Belt. In contrast, Foster *et al.* (1999) interpreted these ages as recording episodes of new mica growth related to uplift of previously deeply buried rocks that were undergoing folding and cleavage formation in the hangingwall of the major décollement. A critical locality to these arguments is the Mt Wellington Fault Zone. As above, $^{40}Ar/^{39}Ar$ ages from this locality were determined on whole-rock slate samples, characterised by highly discordant apparent age spectra. Again, the potential influences of inheritance and recoil need to be evaluated before these ages can be used to constrain the timing of deformation.

Finally, it must be stressed that the above commentary is specific to $^{40}Ar/^{39}Ar$ data from whole-rock low-grade pelites and may not be applicable to results from mica/sericite separates (Foster *et al.* 1998).

Problems with dating regional deformations and the 'Lachlan Orogeny'

The duration of time necessary to develop penetrative structures in rocks such as folds and related cleavage is often difficult to assess. In one study Pfiffner and Ramsay (1982) collated results from relatively young orogenic zones and found that a maximum of deformation phases involving penetrative deformation occurred in an interval of 1–5 million years (see also Paterson & Tobisch 1992). They inferred from measured strain rates that penetrative deformation could develop in intervals as little as 100 000 years. In an example from California, Tavarnelli and Holdsworth (1999) documented four phases of episodic deformation that developed over an interval of 30 million years and produced four sets of coplanar structures.

Along the south coast of NSW, regional unconformities precisely constraining the duration of the regional north–south deformation are lacking and the possibility therefore arises that several different short-duration deformations of similar orientations have been lumped into the one deformation episode. Some authors have supported the notion that the overall complex deformation history of the Lachlan Fold Belt reflects more-or-less continuous orogeny synchronous with sedimentation from latest Ordovician to Late Devonian times (Cas 1983; Powell 1983; Gray *et al.* 1997). VandenBerg (1999) has argued the case for episodic deformation as opposed to continuous deformation on the basis of regional constraints and a reinterpretation of $^{40}Ar/^{39}Ar$ plateau ages of Foster *et al.* (1998). The fact is that in many cases the limits of contractional deformation remain and will continue to remain poorly constrained. Presently the $^{40}Ar/^{39}Ar$ age database is insufficiently accurate to resolve the argument between an episodic interpretation of contractional deformation as opposed to a continuous 'Lachlan Orogeny'.

The way forward

In spite of the many problems associated with determining accurate ages of deformation/metamorphism from low-grade pelites, there are potential solutions. Several studies confirm that recoil and illite inheritance problems are much reduced for epizonal slates (IC <0.25). Therefore, the routine acquisition of illite crystallinity values for slate samples would improve the chances of selecting higher grade samples, which can then be evaluated for potential inheritance problems. For lower grade slates, Dong *et al.* (1995, 1997) have suggested that 'retention ages' from vacuum encapsulation experiments on 0.2 μm clay fractions are more consistent with stratigraphic constraints than either K–Ar ages or total-gas $^{40}Ar/^{39}Ar$ encapsulation ages. ('Retention ages' are determined from $^{40}Ar/^{39}Ar$ step-heating analyses of vacuum-encapsulated clay samples, in which the ^{39}Ar recoil gas is not added to the total-gas ages.)

CONCLUSIONS

New $^{40}Ar/^{39}Ar$ and K–Ar whole-rock ages place an upper constraint of *ca* 440 Ma on the regional deformation of the subduction complex in the Batemans Bay region in the eastern extremity of the Lachlan Fold Belt. This result is more consistent with previously established regional criteria that indicate deformation in the interval 420–410 Ma (Powell 1983). Muscovite inheritance and recoil artefacts are established for all Batemans Bay slate samples, indicating that these problems may be more widespread in the Lachlan Fold Belt than previously recognised (Foster *et al.* 1998, 1999). We suggest that much more caution needs to be applied to the interpretation of $^{40}Ar/^{39}Ar$ ages from Ordovician pelites and that allowances for inheritance and ^{39}Ar recoil should be made in the interpretation of this data.

ACKNOWLEDGEMENTS

This work was funded by an Australian Research Council small grant (number A39130257) and the University of Wollongong (GEME Research Centre). Irradiations in HIFAR nuclear reactor were facilitated by the Australian Institute of Nuclear Science and Engineering and the Australian Nuclear Science and Technology Organisation. Age spectra were plotted using the Isoplot software package of K. Ludwig. We thank David Carrie, Richard Miller and Penny Williamson for technical assistance. We acknowledge useful discussions with David Foster, David Gray, Robin Offler, Jim Dunlap, Paul Carr and John Head. We also thank Jim Dunlap and Robin Offler for comments on the manuscript prior to submission and Ian McDougall and Peter Cawood for helpful reviews.

REFERENCES

Arnaud N. O. & Kelley S. P. 1995. Evidence for excess argon during high pressure metamorphism in the Dora Maira Massif (western Alps, Italy), using an ultra-violet laser ablation microprobe ^{40}Ar–^{39}Ar technique. *Contributions to Mineralogy and Petrology* **121**, 1–11.

Bierlein F. P., Foster D. A., McKnight S. & Arne D. C. 1999. Timing of gold mineralisation in the Ballarat goldfields, central Victoria: constraints from $^{40}Ar/^{39}Ar$ results. *Australian Journal of Earth Sciences* **46**, 301–309.

Bischoff G. C. O. & Prendergast E. I. 1987. Newly discovered Middle and Late Cambrian fossils from the Wagonga Beds of New South Wales, Australia. *Neues Jahrbuch Fur Geologie und Palaontologie* **175**, 39–64.

Cas R. A. F. 1983. A review of the palaeogeography of the Lachlan Fold Belt, southeastern Australia. *Geological Society of Australia Special Publication* **10**.

Dong H., Hall C. M., Halliday A. N., Peacor D. R., Merriman R. J. & Roberts B. 1997. $^{40}Ar/^{39}Ar$ illite dating of Late Caledonian (Acadian) metamorphism and cooling of K-bentonites and slates from the Welsh Basin, U.K. *Earth and Planetary Science Letters* **150**, 337–351.

Dong H., Hall C. M., Peacor D. R. & Halliday A. N. 1995. Mechanisms of argon retention in clays revealed by laser ^{40}Ar–^{39}Ar dating. *Science* **267**, 355–359.

Dong H., Hall C. M., Peacor D. R., Halliday A. N. & Peavear D. R. 2000. Thermal $^{40}Ar/^{39}Ar$ separation of diagenetic from detrital illitic clays in Gulf Coast shales. *Earth and Planetary Science Letters* **175**, 309–325.

Dunlap W. J. 1997. Neocrystallisation or cooling? $^{40}Ar/^{39}Ar$ ages of white micas from low-grade mylonites. *Chemical Geology* **143**, 181–203.

Fergusson C. L. & Tye S. C. 1999. Provenance of Early Palaeozoic sandstones, southeastern Australia, part 1: vertical changes through the Bengal fan-type deposit. *Sedimentary Geology* **125**, 135–151.

Foster D. A., Gray D. R. & Bucher M. 1999. Chronology of deformation within the turbidite-dominated Lachlan Fold Belt: implications for the tectonic evolution of eastern Australia and Gondwana. *Tectonics* **18**, 452–485.

Foster D. A., Gray D. R., Kwak T. A. P. & Bucher M. 1998. Chronology and tectonic framework of turbidite-hosted gold deposits in the western Lachlan Fold Belt, Victoria: ^{40}Ar–^{39}Ar results. *Ore Geology Reviews* **13**, 229–250.

Frikken P. 1997. The stratigraphy and structure of the Early Palaeozoic succession—Burrewarra Point, southeastern NSW. BSc (Hons) thesis, University of Wollongong, Wollongong (unpubl.).

Gaber L. J., Foland K. A. & Corbato C. E. 1988. On the significance of argon release from biotite and amphibole during $^{40}Ar/^{39}Ar$ vacuum heating. *Geochimica et Cosmochimica Acta* **52**, 2457–2465.

Gray D. R. & Foster D. A. 1997. Orogenic concepts—application and definition: Lachlan Fold Belt, eastern Australia. *American Journal of Science* **297**, 859–891.

Gray D. R., Foster D. A. & Bucher M. 1997. Recognition and definition of orogenic events in the Lachlan Fold Belt. *Australian Journal of Earth Sciences* **44**, 489–501.

Hunziker J. C., Frey M., Clauer N., Dallmeyer R. D., Friedrichsen H., Flehmig W., Hochstrasser K., Roggwiler P. & Schwander H. 1986. The evolution of illite to muscovite: mineralogical and isotopic data from the Glarus Alps, Switzerland. *Contributions to Mineralogy and Petrology* **92**, 157–180.

Jenkins C. J., Kidd P. R. & Mills K. J. 1982. Upper Ordovician graptolites from the Wagonga Beds near Batemans Bay, New South Wales. *Journal of the Geological Society of Australia* **29**, 367–373.

Kisch H. J. 1991. Illite crystallinity: recommendations on sample preparation, X-ray diffraction settings, and interlaboratory standards. *Journal of Metamorphic Geology* **9**, 665–670.

Lee J. K. W., Onstott T. C., Cashman K. V., Cumbest R. J. & Johnson D. 1991. Incremental heating of hornblende in vacuo: implications for $^{40}Ar/^{39}Ar$ geochronology and the interpretation of thermal histories. *Geology* **19**, 872–876.

Leitch E. C. & McDougall I. 1979. The age of orogenesis in the Nambucca Slate Belt: a K–Ar study of low-grade regional metamorphic rocks. *Journal of the Geological Society of Australia* **26**, 111–119.

Lewis P. C., Glen R. A., Pratt G. W. & Clarke I. 1994. *Bega–Mallacoota 1:250 000 Geological Sheet SJ/55–4, SJ/55–8: Explanatory Notes*. Geological Survey of New South Wales, Sydney.

Lo C-H., Lee J. K. W. & Onstott T. C. 2000. Argon release mechanisms of biotite in vacuo and the role of short-circuit diffusion and recoil. *Chemical Geology* **165**, 135–166.

Lo C-H. & Onstott T. C. 1989. ^{39}Ar recoil artefacts in chloritised biotite. *Geochimica et Cosmochimica Acta* **53**, 2697–2711.

McDougall I. 1985. K–Ar and $^{40}Ar/^{39}Ar$ dating of the hominid-bearing Pliocene–Pleistocene sequence at Koobi Fora, Lake Turkana, northern Kenya. *Geological Society of America Bulletin* **96**, 159–175.

McDougall I. & Harrison T. M. 1999. *Geochronology and Thermochronology by the $^{40}Ar/^{39}Ar$ Method* (2nd edition). Oxford University Press, New York.

McDougall I. & Roksandic Z. 1974. Total fusion $^{40}Ar/^{39}Ar$ ages, HIFAR reactor. *Journal of the Geological Society of Australia* **21**, 81–89.

Miller J. M. & Gray D. R. 1996. Structural signature of sediment subduction–accretion in a Palaeozoic accretionary complex, southeastern Australia. *Journal of Structural Geology* **18**, 1245–1258.

Miller J. McL. & Gray D. R. 1997. Subduction-related deformation and the Narooma anticlinorium, eastern Lachlan Fold Belt, southeastern New South Wales. *Australian Journal of Earth Sciences* **44**, 237–251.

Offler R., Miller J. McL., Gray D. R., Foster D. A. & Bale R. 1998. Crystallinity and b0 spacing of K-white micas in a Paleozoic accretionary complex, eastern Australia: metamorphism, paleogeotherms, and structural style of an underplated sequence. *Journal of Geology* **106**, 495–509.

Onstott T. C., Mueller C., Vroluk P. J. & Pevear D. R. 1997. Laser $^{40}Ar/^{39}Ar$ microprobe analyses of fine-grained illite. *Geochimica et Cosmochimica Acta* **61**, 3851–3861.

Paterson S. R. & Tobisch O. T. 1992. Rates of processes in magmatic arcs: implications for the timing and nature of pluton emplacement and wall rock deformation. *Journal of Structural Geology* **14**, 291–300.

Pevear D. R. 1992. Illite age analysis, a new tool for basin thermal history analysis. *In*: Kharaka Y. K. & Maest A. ed. *Proceedings of the 7th Symposium on Water–Rock Interactions*, pp. 1251–1254. Balkema, Rotterdam.

Pfiffner O. A. & Ramsay J. G. 1982. Constraints on geological strain rates: arguments from finite strain states of naturally deformed rocks. *Journal of Geophysical Research* **87**, 311–321.

Phillips D. 1991. Argon isotope and halogen chemistry of phlogopite from South African kimberlites: a combined step-heating, laser-probe, electron microprobe and TEM study. *Chemical Geology (Isotope Geoscience Section)* **87**, 71–89.

Phillips D. & Onstott T. C. 1989. Argon isotopic zoning in mantle phlogopite. *Geology* **16**, 542–546.

POWELL C. McA. 1983. Geology of the New South Wales South Coast and adjacent Victoria with emphasis on the pre-Permian structural history. *Geological Society of Australia, Specialist Group in Tectonics and Structural Geology Field Guide* **1**.

POWELL C. McA. 1984. Ordovician to earliest Silurian: marginal sea and island arc; Silurian to mid Devonian dextral transtensional margin; Late Devonian and Early Carboniferous: continental magmatic arc along the eastern edge of the Lachlan Fold Belt. *In*: Veevers J. J. ed. *Phanerozoic Earth History of Australia*, pp. 290–340. Clarendon Press, Oxford.

POWELL C. McA., COLE J. P. & CUDAHY T. J. 1985. Megakinking in the Lachlan Fold Belt. *Journal of Structural Geology* **7**, 281–300.

POWELL C. McA. & RICKARD M. R. 1985. Significance of the early foliation at Bermagui, N.S.W., Australia. *Journal of Structural Geology* **7**, 385–400.

RENNE P., SWISHER C. C., DEINO A. L., KARNER D. B. V., OWENS T. L. & DEPAOLO D. J. 1998. Intercalibration of standards, absolute ages and uncertainties in $^{40}Ar/^{39}Ar$ dating. *Chemical Geology* **145**, 117–152.

REUTER A. & DALLMEYER R. D. 1989. K–Ar and $^{40}Ar/^{39}Ar$ dating of cleavage formed during very low-grade metamorphism: a review. *In*: Daly J. S., Cliff R. A. & Yardley B. W. D. eds. *Evolution of Metamorphic Belts*, pp. 161–171. Geological Society of London Special Publication **43**.

SLETTEN V. W. & ONSTOTT T. C. 1998. The effect of the instability of muscovite during in vacuo heating on $^{40}Ar/^{39}Ar$ step-heating spectra. *Geochimica et Cosmochimica Acta* **62**, 123–141.

STEIGER R. H. & JÄGER E. 1977. Subcommission on geochronology: convention on the use of decay constants in geo- and cosmochronology. *Earth and Planetary Science Letters* **36**, 359–362.

STEWART I. R. & GLEN R. A. 1991. New Cambrian and Early Ordovician ages from the New South Wales south coast. *Geological Survey of New South Wales Quarterly Notes* **85**, 1–8.

TAVARNELLI E. & HOLDSWORTH R. E. 1999. How long do structures take to form in transpression zones? A cautionary tale from California. *Geology* **27**, 1063–1066.

TETLEY N., MCDOUGALL I. & HEYDEGGER H. R. 1980. Thermal neutron interferences in the $^{40}Ar/^{39}Ar$ dating technique. *Journal of Geophysical Research* **85**, 7201–7205.

TUCKER R. D., BRADLEY D. C., VER STRAETEN C. A., HARRIS A. G., EBERT J. R. & MCCUTCHEON S. R. 1998. New U–Pb zircon ages and the duration and division of Devonian time. *Earth and Planetary Science Letters* **158**, 175–186.

TURNER G. & CADOGAN P. H. 1974. Possible effects of ^{39}Ar recoil in ^{40}Ar–^{39}Ar dating. *In*: *Proceedings of the Fifth Lunar Conference* **2**, 1601–1615.

TURNER S. P., KELLEY S. P., VANDENBERG A. H. M., FODEN J. D., SANDIFORD M. & FLÖTTMANN T. 1996. Source of the Lachlan fold belt flysch linked to convective removal of the lithospheric mantle and rapid exhumation of the Delamerian–Ross fold belt. *Geology* **24**, 941–944.

VANDENBERG A. H. M. 1999. Timing of orogenic events in the Lachlan Orogen. *Australian Journal of Earth Sciences* **46**, 691–701.

WRIGHT T. O. & DALLMEYER R. D. 1991. The age of cleavage development in the Ross orogen, northern Victoria Land, Antarctica: evidence from $^{40}Ar/^{39}Ar$ whole-rock slate ages. *Journal of Structural Geology* **13**, 677–690.

WYBORN D. & OWEN M. 1986. *1:100 000 Geological Map Commentary Araluen New South Wales*. Bureau of Mineral Resources, Canberra.

Received 3 October 2000; accepted 8 February 2001